

Distributed vorticity model for vortex molecule dynamics

Sarthak Choudhury¹ and Joachim Brand¹

¹*Dodd-Walls Centre for Photonic and Quantum Technologies,
New Zealand Institute for Advanced Study, Centre for Theoretical Chemistry and Physics,
Massey University, Auckland 0632, New Zealand*

(Dated: December 15, 2022)

We analyze the effect of a hard wall trapping potential on the dynamics of a vortex molecule in a two-component Bose-Einstein condensate with linear coherent coupling. A vortex molecule consists of a vortex of the same charge in each component condensate connected by a domain wall of the relative phase. In a previous paper [Phys. Rev. A 106, 043319] we described the interaction of a vortex molecule with the boundary using the method of images by separately treating each component vortex as a point vortex, in addition to a Magnus force effect from the surface tension of the domain wall. Here we extend the model by considering a continuous distribution of image vorticity reflecting the effect of the domain wall on the vortex molecule phase structure. In the case of a precessing centered vortex molecule in an isotropic trap, distributing the image vorticity weakens its contribution to the precession frequency. We test the model predictions against numerical simulations of the coupled Gross-Pitaevskii equations in a two-dimensional circular disc and find support for the improved model.

Keywords: coherently coupled superfluids, fractional vortex molecule, coreless vortex, Josephson vortex

I. INTRODUCTION

The quantization of vortex lines is a striking feature of superfluids that appears as a consequence of Bose-Einstein condensation [1]. The dynamics of superfluid vortices still poses many open questions and is actively pursued [2–5]. Shortly after the first observation of quantized vortices in a dilute gas Bose-Einstein condensate (BEC) [6], experiments introduced coherent coupling in multi-component BECs by applying a radio-frequency electromagnetic field that drives a Rabi transition between internal (hyperfine) states in the constituent atomic gas [7], with more refined experiments becoming available recently [8–10]. Theoretical work then examined the peculiar structure of vortices in such a two-component BEC under the continuous influence of coherent coupling [11, 12]. Due to the coherent coupling, the phases of the component condensates are not independent. Instead the phases align in equilibrium. As a consequence, vortices in the component BECs have to be connected by a vortex line that extends between the two BECs as a domain wall of the relative phase, also known as a Josephson vortex. Analytic solutions for stationary Josephson vortices were first found by Kaurov and Kuklov [13, 14], and families of moving Josephson vortices were characterized in Ref. [15].

Domain walls have an energy content, or surface tension, which is approximately linear in their extent, i.e. length in two dimensions and area in three dimensions. This makes them susceptible to breaking up into smaller fragments. Their dynamical stability is determined by the sign of their effective mass, which depends on the competition between the Rabi coupling and the nonlinear mean-field energy in the BECs [15–17]. Interesting analogies to axions and quark confinement were first pointed out by Son and Stephanov [11] (see also

[18–20]).

In two-dimensional BECs, a domain wall can either terminate at a boundary of the superfluid domain, or at an appropriately charged vortex in either of the component BECs. A configuration with same-charge vortices in each component connected by a domain wall is known as a vortex molecule [21]. Sometimes it is referred to as fractional vortex molecule to highlight the fact that the quantized vortex charge can be thought of as being split into fractional charges residing in separate locations at the vortices in each component BEC [22]. Theoretical studies of equilibrium configurations have been extended to vortex molecule lattices [23].

The dynamics of vortex molecules has first been considered by Tylutki *et al.* [24] in the context of a two-dimensional coupled BEC in an isotropic harmonic trap. In this scenario a symmetrically centered vortex molecule rotates with a constant angular frequency around the trap axis, referred to as precession. The vortex molecule dynamics was described by the superposition of three separate velocity components: One derived from the influence of the harmonic trapping potential on the individual (point) vortices in a Thomas Fermi approximation, and two contributions from the Magnus effect related to a short-range core repulsion and an attraction due to the surface tension of the domain wall. Calderaro *et al.* [25] then developed a Lagrangian variational formalism focussing on the effect of the domain wall on the vortex dynamics. They obtained analytic results in two different regimes: The attractive Magnus force is linear in the molecular distance d (the length of the domain wall) in the regime of weak Rabi coupling where $\xi_J \gg d \gg \xi$, and ξ_J is the Josephson vortex length scale (width of the domain wall), and ξ is the condensate healing length. In this regime, the Magnus force contribution to the precession frequency is constant. The other regime of strong Rabi coupling where $d \gg \xi_J \gg \xi$ is the one considered

by Tylutki *et al.* [24] where the Magnus force is constant and provided by the surface tension of an infinite domain wall.

In a previous work we developed an extended point vortex model to analyze the dynamics of a vortex molecule in a flat-bottom trap realizing a channel geometry with parallel hard walls [26]. The model includes the Magnus-force effects of the domain wall and possible core repulsion by parameterizing a numerically-obtained vortex-vortex interaction energy in the absence of domain boundaries. The effects of the hard-wall boundaries are separately taken into account by the method of images applied on the individual component vortices. This theory was able to predict all the qualitative features in the pendulum-like phase space of the vortex molecule dynamics in the channel geometry of Ref. [26].

In this work we aim for a more accurate description of the vortex-molecule dynamics in the presence of domain boundaries. Instead of treating the component vortices as point vortices, we consider the vorticity to be distributed along the domain wall connecting the component vortices for the purpose of generating image vorticity. This is motivated by the fact that over length scales larger than the molecular separation and the Josephson length scale, the phase of both condensate components aligns and resembles that of a distributed vorticity rather than a point vortex.

Magnus-force contributions from the domain-wall surface tension and core-interaction are obtained from the numerically generated vortex-molecule interaction energy as in our previous work [26]. For the current work we use a more accurate representation of the numerical data compared to the parameterization used in Ref. [26], which we found necessary in order to obtain quantitative agreement with fully numerical simulations of the vortex molecule dynamics.

We derive and solve the equations of motion for the distributed vorticity model for the case of a single vortex molecule in a disc shaped domain with hard wall boundary conditions. This situation could be achieved in BEC experiments with a flat-bottom trap. The model solutions are compared with fully numerical solutions of the Gross-Pitaevskii equation (GPE). We also compare with the simpler method of images for point vortices and a simplified description of the surface tension that is linear in the domain wall size and find that the refined model gives the best agreement with the GPE data.

The paper is structured as follows. Section II introduces the coupled GPE governing the system of coherently coupled condensates. Section III introduces the point vortex formulation and recapitulates the extended point vortex model before defining the distributed vorticity model. The general formulations are applied to the dynamics of a vortex molecule in a flat-bottom trap in Sec. IV before concluding in Sec. V. Appendix A provides relevant details of the interaction energy which has been appropriately parametrized and Appendix B discusses the calculation of the general integrals of the charge dis-

tribution model.

II. MEAN-FIELD FORMULATION

We characterize two coherently coupled atomic Bose-Einstein condensates with complex order parameters, $\psi_1(\mathbf{r}, t)$ and $\psi_2(\mathbf{r}, t)$ in the mean-field description of coupled GPEs

$$i\hbar \frac{d\psi_1}{dt} = \left(\hat{h} - \mu + g_1 |\psi_1|^2 + g_{12} |\psi_2|^2 \right) \psi_1 - \nu \psi_2, \quad (1a)$$

$$i\hbar \frac{d\psi_2}{dt} = \left(\hat{h} - \mu + g_2 |\psi_2|^2 + g_{12} |\psi_1|^2 \right) \psi_2 - \nu \psi_1, \quad (1b)$$

where $\hat{h} = -\frac{\hbar^2}{2m} \nabla^2 + V_{\text{ext}}$ is the single-particle Hamiltonian for bosons of mass m . The chemical potential given by μ controls the number of particles in numerical simulations. The spatially homogeneous coherent (Rabi) coupling ν can be realized by a two photon microwave field or a driving radio frequency. The atoms are assumed to be strongly confined along the z spatial dimension to realize a quasi two dimensional quantum gas with a positional coordinate denoted as $\mathbf{r} = (x, y)^t$. Additional box-like confinement in the two-dimensional plane is provided by the external potential $V_{\text{ext}}(\mathbf{r})$, which we take to vanish inside the superfluid domain and rising sharply at the domain boundaries. This will create a uniform quasi-two-dimensional Bose-Einstein condensate with rigid (hard-wall) boundaries as realized, e.g., in Ref. [27].

Our zero temperature theory is applicable to the low temperature and high particle-number-density regime of experiments [27]. The free energy associated with the GPE (1) is given by the integral

$$W = \int \left[\sum_{i=1}^2 \left(\psi_i^* \hat{h} \psi_i + \frac{g_i}{2} |\psi_i|^4 - \mu |\psi_i|^2 \right) + g_{12} |\psi_1|^2 |\psi_2|^2 - \nu (\psi_1^* \psi_2 + \psi_1 \psi_2^*) \right] d^2r. \quad (2)$$

We are interested in the miscible regime where $g_{12}^2 < g_1 g_2$ and choose equal intra-component interactions $g_1 = g_2 \equiv g$ in order to reduce the number of parameters. The homogeneous and time-independent ground-state solution of Eq. (1) for $V_{\text{ext}} = 0$ is given by equal and constant density $|\psi_{1/2}|^2 = (\mu + \nu)/(g + g_{12}) \equiv n_0$ in the component condensates. This serves as the background bulk density for localized vortex or non-linear-wave solutions. The linear coupling $\nu > 0$ ensures that component condensates phases align and thus $\psi_1 = \psi_2$ in equilibrium, but a global phase factor remains undetermined due to a global $U(1)$ symmetry of the coupled BECs. The healing length

$$\xi = \frac{\hbar}{\sqrt{m(g + g_{12})n_0}} = \frac{\hbar}{\sqrt{m(\mu + \nu)}} \quad (3)$$

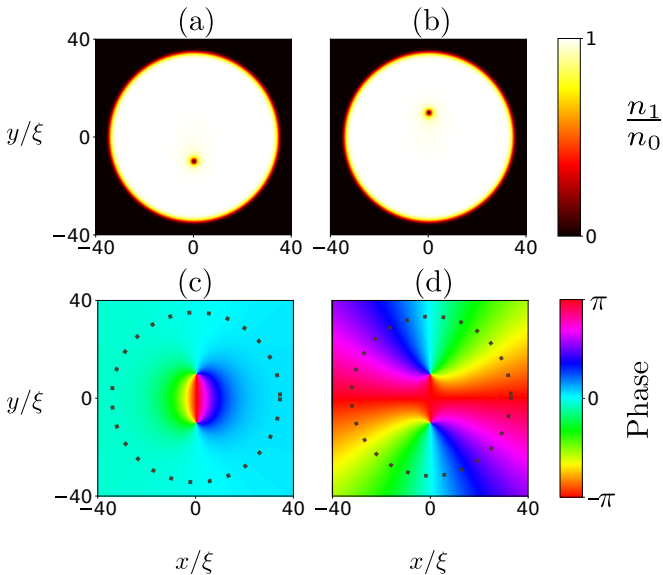


Figure 1. Vortex molecule in a disc. Numerical solution of the GPE (1) with a centered vortex molecule with molecular length $d = 20\xi$ in a disc-like trap described by Eq. (5). (a) Density of condensate 1, $n_1 = |\psi_1|^2$. (b) Density of condensate 2, $n_2 = |\psi_2|^2$. (c) Relative phase $\arg(\psi_1\psi_2^*)$. (d) Total phase $\arg(\psi_1\psi_2)$. The black dotted lines in panels (c) and (d) denote the trap boundary at $L = 35\xi$. Other parameters are $\nu = 2 \times 10^{-3}\mu$, $g = \mu\xi^2$, $g_{12} = 0$.

provides the length scale on which a homogeneous solution is recovered away from forced local inhomogeneities due to vortex cores, or boundary conditions [28].

A point vortex model, nominally applicable to an incompressible fluid, requires that the healing length is smaller than other relevant length scales like the separation of vortices, or the distance of vortices from the boundaries [29, 30]. Reference [31] showed how to relax the incompressibility condition of the point vortex model and obtain correction terms for vortex dynamics as a power series in ξ/L , where L is a length scale of the superfluid domain. Vortex molecules introduce two additional length scales on top of the healing length. The molecular size d is the separation between the vortex singularities in the component vortices and also determines the length of the domain wall in the relative phase in situations where the domain wall extends along a straight line connecting the component vortices. The third length scale

$$\xi_J = \frac{\hbar}{4m\nu}, \quad (4)$$

is called the Josephson vortex length scale and determines the width of the domain wall connecting the two component vortices. Exact solutions for a stationary and moving Josephson vortex were characterized in Refs. [13] and [15], respectively.

Figure 1 illustrates a vortex molecule solution of the coupled GPE (1) in a disc-shaped two-component BEC.

The disc shaped radially symmetric external potential of radius L is described by

$$V_{\text{ext}}(\mathbf{r}) = (\mu + \nu) \left(1 + \tanh \frac{|\mathbf{r}| - L}{\xi} \right). \quad (5)$$

The solution shown in Fig. 1 was obtained by first imprinting a single vortex in each condensate component at the desired locations $\mathbf{R}_1, \mathbf{R}_2$. A low energy solution is then obtained by evolving Eq. (1) in imaginary time, i.e. replacing $t \rightarrow -i\tau$, which corresponds to minimizing the energy functional W by gradient flow. Imaginary time evolution quickly removes most density and non-topological phase excitations. On a slower timescale, the location of vortex phase singularities move towards lower energy configurations, which eventually moves them outside the trap. To avoid this, Gaussian pinning potentials are used to pin the vortices in a particular configuration for each vortex while only having minimal effect on the phase and density structure. While the obtained solutions are stationary only in the presence of the pinning potential, they also serve as suitable initial conditions for studying vortex dynamics under real-time evolution of the coupled GPE (1) when the pinning potentials are removed. Under the assumptions of the point vortex model, the vortex dynamics only depends on the instantaneous position of the vortex singularities by evolving through minimal energy configurations. We test the predictions of the point vortex model by comparing with fully time-dependent GPE dynamics. Vortex positions are tracked by accurately locating the phase singularities using the software library `VortexDistributions.jl` [32].

III. POINT VORTEX FORMULATION

The idea of the point vortex model is that the dynamics of vortices is fully determined by the positions of all vortices in the system together with the boundary conditions. The model strictly applies to ideal inviscid and incompressible fluids [29, 33], and can be applied to the GPE in situations where the healing length ξ can be considered a small parameter [30, 31]. For an ideal fluid in two dimensions one can define a scalar stream function whose contours are co-linear with the local fluid velocity $\mathbf{u}(\mathbf{r})$. The velocity of a point vortex at position \mathbf{R} can be found from the stream function after the singular contribution of the vortex itself has been removed [33]. While the stream function cannot be used for multi-component coupled BECs, an alternative approach based on energy conservation is still applicable.

The idea is to find the point vortex trajectories as the contours of a conserved energy function, which only depends on the vortex coordinates after the boundary conditions are defined. This leads to a Hamiltonian formulation where the vortex x and y coordinates play the role of canonically conjugate variables. In this formulation ad-

ditive contributions to the total energy provide additive contributions to the vortex velocity.

A. Extended point vortex model for the vortex molecule

In Ref. [26] we presented an extended point vortex model where the total energy of a vortex molecule is given by

$$E_{\text{vm}}(\mathbf{R}_1, \mathbf{R}_2) = E_{\text{bound}}(\mathbf{R}_1, \mathbf{R}_2) + V(|\mathbf{R}_1 - \mathbf{R}_2|), \quad (6)$$

where $\mathbf{R}_j = (X_j, Y_j)^t$ is the coordinate vector of the j th component vortex, $E_{\text{bound}}(\mathbf{R}_1, \mathbf{R}_2)$ is an energy contribution from the boundary-induced image vortices, and $V(d)$ is an internal energy of the vortex molecule that only depends on the separation of the component vortices, or the molecular size, $d = |\mathbf{R}_1 - \mathbf{R}_2|$. The trajectories of the component vortices are then obtained from the equation of motion

$$\dot{\mathbf{R}}_j = \nabla_j^\perp \frac{E_{\text{vm}}(\mathbf{R}_1, \mathbf{R}_2)}{2\pi n_0 \kappa}, \quad (7)$$

$$(8)$$

where $\kappa = \pm 1$ is the integer vortex charge and

$$\nabla_j^\perp = \begin{pmatrix} \frac{\partial}{\partial Y_j} \\ -\frac{\partial}{\partial X_j} \end{pmatrix} \quad (9)$$

is the projection of the curl onto the x - y plane. The equation of motion (7) has the structure of Hamilton's equations of motion common to the Hamiltonian formulation of point vortex dynamics [33]. As a consequence of the two energy contributions of Eq. (6) the equation of motion has two contributions to the point vortex velocity:

$$\dot{\mathbf{R}}_j = \mathbf{V}_j^{\text{bound}} + \mathbf{V}_j^{\text{int}}. \quad (10)$$

Reference [26] made specific assumptions for the two terms in Eq. (6): The boundary term was provided by the method of images for each component vortex separately

$$E_{\text{bound}}(\mathbf{R}_1, \mathbf{R}_2) = E_{\text{sv}}(\mathbf{R}_1) + E_{\text{sv}}(\mathbf{R}_2), \quad (11)$$

where $E_{\text{sv}}(\mathbf{R})$ is the energy contribution of a single vortex in the superfluid within the given boundaries, i.e. incorporating the contributions from image vortices. As a consequence, the point vortex velocity contributions in the equation of motion become

$$\mathbf{V}_j^{\text{bound}} = \mathbf{V}_j^{\text{sv}} \equiv (2\pi n_0 \kappa)^{-1} \nabla^\perp E^{\text{sv}}(\mathbf{R})|_{\mathbf{R}=\mathbf{R}_j} \quad (12)$$

$$\mathbf{V}_j^{\text{int}} = (2\pi n_0 \kappa)^{-1} \frac{dV(d)}{dd} \nabla_j^\perp |\mathbf{R}_1 - \mathbf{R}_2|. \quad (13)$$

The interaction energy $V(d)$ was parameterized from a numerical calculation of the vortex-molecule energy in

the absence of boundaries. This model provided an adequate description of the dynamics of the vortex molecule in a channel with parallel side wall and was able to reproduce all qualitative phase space structures in Ref. [26].

We note, however, that this model is too simplistic for a fully quantitative description of vortex-molecule dynamics. In particular, the velocity contribution of the boundary term \mathbf{V}_j^{sv} originates from the image vortices of the component vortex at position \mathbf{R}_j only. We know however that the phase structure of the component condensates is not independent of each other but rather strongly influenced by the Rabi coupling. A domain wall of the relative phase extends between the component vortices roughly along the molecular axis. At distances larger than ξ_J away from the domain wall, the relative phase drops to zero and the phases of each component BECs align, see Fig. 1.

This observation motivates us to modify the extended point vortex model by considering an image vortex distribution extended along the image of the domain wall of the relative phase. For this work we retain the formulation of the extended point vortex model of Eqs. (6) and (7), but improve the approximate representation of the two energy terms. For the interaction energy $V(d)$ we use a more accurate numerical representation based on the same numerical calculation as detailed in Appendix A. An improved representation of the boundary contributions to the vortex molecule equation of motion is the subject of the distributed vorticity model.

B. Distributed vorticity model

Due to the effect of the boundaries each vortex obtains a velocity component that can be thought of as the linear superposition of velocity fields induced by all image vortices at the position of that vortex. Let

$$\kappa \mathbf{u}_{\text{im}}(\mathbf{r}; \mathbf{R}) \quad (14)$$

denote the velocity field induced by the images of a vortex at position \mathbf{R} with charge κ . The boundary-induced velocity contribution in the extended point vortex model of Sec. III A of vortex j then becomes

$$\mathbf{V}_j^{\text{sv}} = \kappa \mathbf{u}_{\text{im}}(\mathbf{R}_j; \mathbf{R}_j). \quad (15)$$

For the distributed vorticity model we take the source of image vorticity to be distributed along the domain wall of the relative phase extending between the two component vortices of the vortex molecule, i.e. along the molecular axis. Thus the velocity component of vortex j originating from the image vorticity becomes a superposition of velocity contributions

$$\mathbf{V}_j^{\text{dv}} = \kappa \int_0^1 \mathbf{u}_{\text{im}}(\mathbf{R}_j; (1-t)\mathbf{R}_1 + t\mathbf{R}_2) dt. \quad (16)$$

Figure 2 is a concept diagram that shows how the distributed vorticity of the vortex molecule can be thought

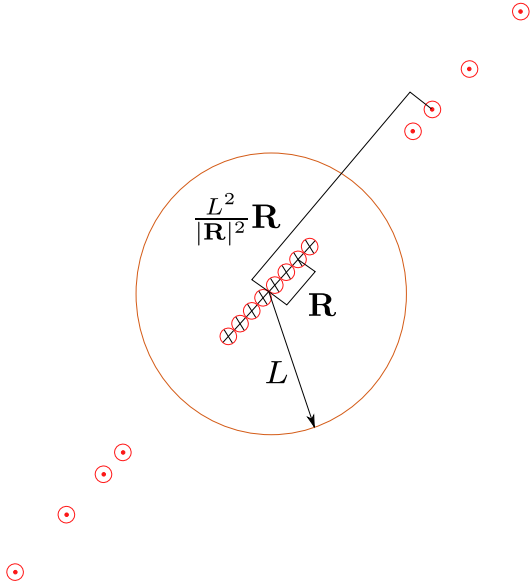


Figure 2. Concept diagram of the vorticity distribution model for a centered vortex molecule in a disc trap. The image vortices are formed at locations $\tilde{\mathbf{R}} = \frac{L^2}{|\mathbf{R}|^2} \mathbf{R}$ where \mathbf{R} is the position of the original charge. The distance of the image vortices from the center of the condensate is inversely proportional to the distance of its original vortex from the center. Hence, even though the charge distribution is evenly spaced the image charges are not and reach out to infinity as $|\mathbf{R}| \rightarrow 0$.

of as being composed of individual vortices of fractional charge, giving rise to a distribution of image vortices in turn. In the following we will apply these ideas to the disc geometry.

IV. VORTEX MOLECULE DYNAMICS IN A FLAT-BOTTOM DISC TRAP

A. Velocity of a simple vortex in a disc

The simple vortex solution can be understood as a special case of a vortex molecule where the two vortices are at the same location. In this case the phase of the two component condensates can align perfectly and thus no domain wall of the relative phase is present. The velocity of the simple vortex in a disc is thus completely determined by the contribution from the boundaries. Moreover, the predictions from the extended point vortex model and from the distributed vorticity model trivially agree and become equivalent to the point vortex model for a single-component superfluid.

In the point vortex model we ignore the compressibility of the superfluid, formally taking $\xi \rightarrow 0$, and assume a constant condensate density. The phase of the GP order parameter of a single vortex at position $\mathbf{R} = (X, Y)^t$ is given by $\arg[\psi(\mathbf{r})] = \kappa \arctan \frac{x-X}{y-Y}$ in the absence of boundaries (up to a constant), and the corresponding ve-

locity field is

$$\mathbf{u}(\mathbf{r}) = \frac{\hbar}{m} \nabla \arg(\psi) = \frac{\hbar \kappa \hat{z} \times (\mathbf{r} - \mathbf{R})}{m |\mathbf{r} - \mathbf{R}|^2}. \quad (17)$$

The influence of the box-like trapping potential is to create a no-flow boundary condition, i.e. a condition that prohibits a perpendicular component of the superfluid velocity distribution at the boundary. For a circular disc centered at the origin with radius L this boundary condition is met by adding an image vortex with charge $-\kappa$ at the position [33]

$$\tilde{\mathbf{R}} = \frac{L^2 \mathbf{R}}{|\mathbf{R}|^2}. \quad (18)$$

The velocity field induced by the image of a vortex with charge κ at position \mathbf{R} is thus

$$\kappa \mathbf{u}_{\text{im}}(\mathbf{r}; \mathbf{R}) = -\frac{\hbar \kappa \hat{z} \times (\mathbf{r} - \tilde{\mathbf{R}})}{m |\mathbf{r} - \tilde{\mathbf{R}}|^2}. \quad (19)$$

The boundary contributions to the velocities of the component vortices in a vortex molecule can now be obtained by substituting Eq. (19) into Eqs. (15) and (16) for the extended point-vortex model and the distributed vorticity models, respectively. The full equation of motion for the vortex molecule is then given by Eq. (10) in combination with Eq. (13).

B. Precession of a centered vortex molecule

In order to quantitatively compare between the different models, we now focus on the situation where the vortex molecule is located symmetrically in the center of the disc with $\mathbf{R}_1 = -\mathbf{R}_2$ and $|\mathbf{R}_j| = d/2$. In this case the symmetry is preserved during the vortex motion. The point vortex velocity is perpendicular to the molecular axis and the vortex molecule rotates with a constant precession frequency around the axis of the disc trap

$$\begin{aligned} \Omega_{\text{vm}} &= \frac{\kappa |\mathbf{V}_j|}{|\mathbf{R}_j|}, \\ &= \Omega_{\text{bound}} + \Omega_{\text{int}}, \end{aligned} \quad (20)$$

which breaks up into components originating from the boundary and interactions as per Eq. (10). The interaction contribution to the precession frequency becomes, from Eq. (13)

$$\Omega_{\text{int}} = \frac{\kappa}{\pi n_0 \hbar d} \frac{dV(d)}{dd}. \quad (21)$$

In a situation where the domain wall energy is purely linear in d , as derived for $d \gg \xi_J$ in Ref. [25], the gradient term is constant and the interaction contribution to the precession frequency becomes inversely proportional to

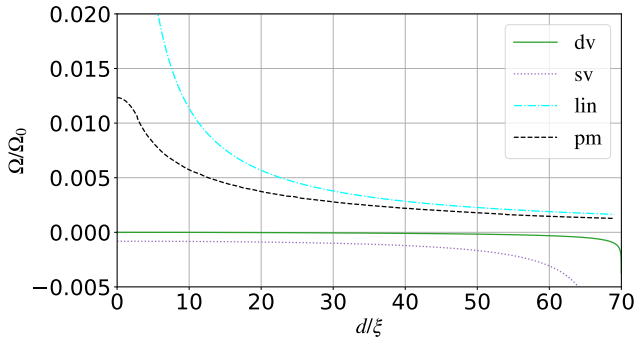


Figure 3. Components of the vortex molecule precession frequency according to various models as a function of the molecular size d . The negative-valued boundary contributions Ω_{bound} are labeled “dv” for the distributed velocity contribution Ω_{dv} of Eq. (23) and “sv” for the single vortex contribution Ω_{sv} of Eq. (22). The interaction components Ω_{int} follow Eq. (21) and bring positive contributions. The one labeled “lin” follows from a purely linear interaction potential with the surface tension of the idealized Josephson vortex. The contribution from the parameterized numerically obtained interaction energy is labelled “pm”. The frequency is expressed in units of $\Omega_0 = (\mu + \nu)/\hbar$. Parameters are same as Fig. 1

the molecular length scale d . This term is divergent for small d .

For the boundary contribution Ω_{bound} we consider the single vortex contribution from the extended point vortex model and the distributed vorticity model. The latter becomes [from Eqs. (15) and (19)]

$$\Omega_{\text{sv}}(d) = -\frac{\hbar\kappa}{m} \frac{4}{4L^2 - d^2}. \quad (22)$$

This is the result of Ref. [26]. Obtaining the former requires evaluating the integral in Eq. (16). A closed form solution can be found and leads to

$$\Omega_{\text{dv}}(d) = \frac{\hbar\kappa}{m} \frac{4}{d^4} \left[d^2 - 2L^2 \ln \left(\frac{4L^2 + d^2}{4L^2 - d^2} \right) \right]. \quad (23)$$

Expanding in powers of d in the vicinity of $d = 0$ we obtain

$$\Omega_{\text{dv}}(d) = -\frac{\hbar\kappa}{m} \frac{d^2}{12L^4} + O(d^6), \quad (24)$$

where the leading term is of second order in d . Thus, the boundary contribution to the precession frequency from the distributed vorticity model vanishes at small molecular size. This is in contrast to the single-vortex contribution from the extended point vortex model of Eq. (22), which has the finite limit $\Omega_{\text{sv}}(0) = -\hbar\kappa/mL$. A comparison of the different contributions to the precession frequency is shown in Fig. 3.

Figure 3 also shows two different curves for Ω_{int} according to different models for the interaction energy of the vortex molecule. The simplest choice with a linear d dependence is

$$V_{\text{lin}}(d) = d\sigma, \quad (25)$$

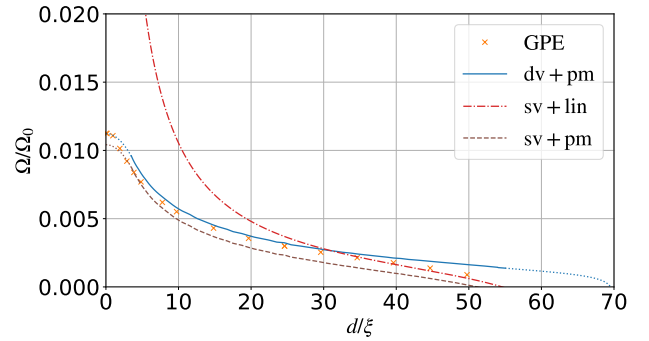


Figure 4. Precession frequency of a centered vortex molecule in a disc trap as a function of the molecular size d . The orange crosses represent real time evolution data from the GPE of Eq. (1). The curves are model predictions according to Eq. (20) with different combinations of the contributions for Ω_{bound} and Ω_{int} shown in Fig. 3. The blue solid line combines the distributed vorticity variant of the boundary contribution with the parametrized interaction energy and provides the best explanation of the numerical GPE data within the available models. The red dot-dashed line represents single vortex boundary contribution from Eq. (22) along with the linear interaction energy contribution from Eq. (25). The brown dashed line represents single vortex boundary contribution along with parameterized interaction energy contribution. The frequency is expressed in units of $\Omega_0 = (\mu + \nu)/\hbar$. Parameters are same as Fig. 1

where

$$\sigma = \frac{8\hbar\sqrt{\nu}}{3\sqrt{m}} \frac{3\mu - \nu}{g + g_{12}}, \quad (26)$$

is the energy (line density) of a Josephson vortex [13], the exact solution for a non-moving domain wall of the relative phase. Reference [24] used this model with an approximate domain wall energy density valid for small ν , which was also derived for $d \gg \xi_J$ in Ref. [25].

As an alternative we have parameterized the numerically computed vortex molecule interaction energy $V_{\text{pm}}(d)$. The numerical calculation of the interaction energy was first reported in Ref. [26]. For the current work we have re-parameterized the numerical data in order to obtain increased accuracy as detailed in App. A. We find that the parameterized numerical interaction energy as well as the derived frequency contribution Ω_{pm} is significantly smaller than the linear model and deviates quite strongly for small and moderate values of d while it asymptotically agrees at large d , as is expected.

In Fig. 4 we show numerical results for the vortex molecule precession frequency from GPE simulations in comparison with model predictions combining different components for the boundary and interaction contributions. For small molecular size d the values of the precession frequency are dominated by the interaction contributions. The linear interaction energy model leads here to a divergent contribution, which unphysical. The parameterized numerical interaction contribution however,

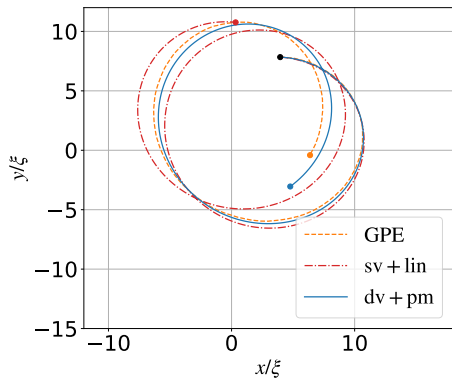


Figure 5. Trajectories predicted for a vortex of an off centered vortex molecule by different models. The starting point for the vortex is (3.95,7.83) marked by the black dot. The other vortex starts at (2.07,-7.71). The color scheme is the same as Fig. 4 and the colored lines represent the predictions from the corresponding models. The colored dots give the endpoint of the different trajectories.

captures the numerically observed finite precession frequency at small molecular sizes rather nicely. While the distributed vorticity and the single vortex contributions for the boundary term only show small differences, the numerical data matches the distributed vorticity model better over the whole range of available data.

Using the non-centered equations for \mathbf{v}_3 and \mathbf{v}_1 , an off-centre trajectory of the vortex molecule is also shown in Fig. 5 with vortex length $d = 16\xi$.

V. CONCLUSION

The predictions of the charge distribution model agree remarkably well with the GPE simulations compared to the extended point vortex model for the centered case for small d . Even in off-centered case as shown in Fig 5, the charge distribution model predicts trajectories which agree with the GPE trajectories to a high degree.

For larger d where the vortex molecule nears the boundaries, the charge distribution model is no longer a valid assumption to make since the total phase can no longer be approximated by our distributed quanta as shown in Fig. 6, even though it still shows better agreement than the single point vortex model.

VI. ACKNOWLEDGEMENTS

Appendix A: Interaction energy

The interaction energy is mainly found as a function of molecular length d by creating a vortex molecule in real projective plane boundary conditions and then using imaginary time evolution of the GPE in Eq. (1) which

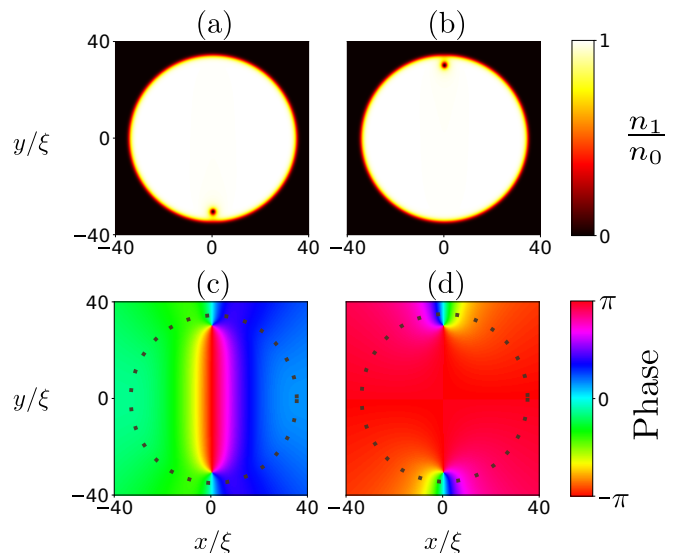


Figure 6. Numerical solution of the GPE with a centered vortex molecule with molecular length= 60ξ . (a) Density of condensate 1 $|\psi_1|^2$. (b) Density of condensate 2 $|\psi_2|^2$. (c) Relative Phase $\arg(\psi_1\psi_2^*)$. (d) Total Phase $\arg(\psi_1\psi_2)$. The black dashed line in (c),(d) denotes the trap boundary at $L = 35$. Other parameters are $\nu = 2 \times 10^{-3}\mu$, $g = \mu\xi^2$.

causes the system to converge to a lower energy state thereby decreasing the molecular length. Further details about this process and the associated boundary conditions can be found in [26]. Here we try to do a more quantitatively accurate fit than in [26] since small deviations in fitting result in large deviations of the derivative and hence in Fig. 4. We plot the interaction energy V as a function of d in Fig. 7 along with 3 different parametrization strategies. The orange dots are given by actual data points from the imaginary time evolution of the GPE. Only representative points are shown. We use a 3rd order spline to parametrize the data given by the blue solid line. Our data extends only up to 55ξ , and we extrapolate beyond that with a linear fit shown by a green dash-dotted using the last 3 spline points since we expect the interaction energy to be linear at length scales much larger than $\xi_J = 11.19\xi$.

The inset shows a closeup for small $d \in [0, 3]$. Imaginary time evolution after decreasing the molecular length to zero starts to make small changes in the overall global phase to decrease the energy. This happens in a much slower timescale than in which the length of the vortex molecule decreases but introduces a difference in slope which is amplified in the precession frequency given by Eq. (21) due to the $1/d$ factor for small d . We expect the interaction energy to plateau for small d and fit a fourth order polynomial discarding the odd orders for small d given by,

$$f(d) = p_1 + p_2 d^2 + p_3 d^4 \quad (\text{A1})$$

where $p_1 = 33.35$, $p_2 = 0.0239$ and $p_3 = -0.000714$ are

the fitting parameters.

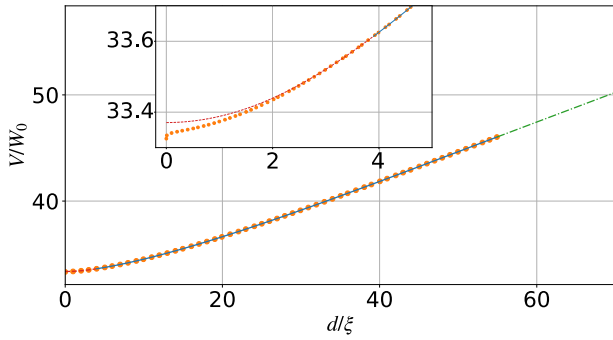


Figure 7. Fitting the interaction energy as a function of molecular length d in units of the healing length ξ . The imaginary time evolution of the GPE and associated boundary conditions to get this data has been discussed in [26]. Inset is a closeup of the for small d . The orange points denote imaginary time evolution data of a vortex molecule in real projective plane boundary conditions. The blue dashed line represents a 3rd order spline that has been fitted to the data. The green dot-dashed line is an extrapolation for large d . The red line denotes a fit that has been done for small d . $W_0 = \hbar^2(\mu + \nu)/m(g + g_{12})$

Appendix B: General integrals of the charge distribution model

The velocity of the vortex at \mathbf{R}_1 in the distributed vorticity model in any arbitrary position of the vortex

molecule is given by Eq. (16) as,

$$\mathbf{V}_1^{\text{dv}}(R_1) = \kappa \int_0^1 \mathbf{u}_{\text{im}}(\mathbf{R}_1; (1-t)\mathbf{R}_1 + t\mathbf{R}_2) dt, \quad (\text{B1})$$

$$= \frac{\hbar\bar{\kappa}}{m} \hat{z} \times [\mathbf{R}_1 I_1 - \mathbf{R}_2 I_2], \quad (\text{B2})$$

where I_1 and I_2 are

$$I_1 = \int_0^1 \frac{\left(1 - \frac{L^2}{R_i^2}\right) + t \frac{L^2}{R_i^2}}{|\mathbf{R}_1 \left(1 - \frac{L^2}{R_i^2}\right) - \frac{L^2}{R_i^2} t \mathbf{d}|^2} dt, \quad (\text{B3})$$

$$I_2 = \int_0^1 \frac{\frac{L^2}{R_i^2} t}{|\mathbf{R}_1 \left(1 - \frac{L^2}{R_i^2}\right) - \frac{L^2}{R_i^2} t \mathbf{d}|^2} dt, \quad (\text{B4})$$

with $\mathbf{d} = \mathbf{R}_2 - \mathbf{R}_1$ and $R_i^2 = |\mathbf{R}_1 + t\mathbf{d}|^2$. The scalar integrals come out as,

$$I_1 = \frac{1}{dR_1^3} \left(dR_1 + L^2 \left\{ \left[\arctan(\cot \theta) - \arctan \left(\cot \theta + \frac{dR_1 \operatorname{cosec} \theta}{R_1^2 - L^2} \right) \right] \cos 2\theta \operatorname{cosec} \theta + \cos \theta \ln \frac{d^2 R_1^2 + (L^2 - R_1^2)^2 + 2dR_1(R_1^2 - L^2) \cos \theta}{(L^2 - R_1^2)^2} \right\} \right), \quad (\text{B5})$$

$$I_2 = \frac{R^2}{2d^2 R_1^2} \left\{ 2 \left[\arctan(\cot \theta) - \arctan \left(\cot \theta + \frac{dR_1 \operatorname{cosec} \theta}{-L^2 + R_1^2} \right) \right] \cot \theta + \ln \frac{d^2 R_1^2 + (L^2 - R_1^2)^2 + 2dR_1(R_1^2 - L^2) \cos \theta}{(L^2 - R_1^2)^2} \right\} \quad (\text{B6})$$

with θ being the angle between \mathbf{R}_1 and \mathbf{d} . I_1 has a removable singularity at $\theta = 0$.

-
- [1] Anthony James Leggett, *Quantum Liquids* (Oxford University Press, Oxford, 2006).
- [2] Xiaoquan Yu and Ashton S. Bradley, “Emergent Non-Eulerian Hydrodynamics of Quantum Vortices in Two Dimensions,” *Phys. Rev. Lett.* **119**, 185301 (2017), [arXiv:1704.05410](#).
- [3] Shaun P. Johnstone, Andrew J. Groszek, Philip T. Starkey, Christopher J. Billington, Tapio P. Simula, and Kristian Helmerson, “Evolution of large-scale flow from turbulence in a two-dimensional superfluid,” *Science* **364**, 1267–1271 (2019).
- [4] W. J. Kwon, G. Del Pace, K. Khani, L. Galantucci, A. Muzi Falconi, M. Inguscio, F. Scazza, and G. Roati, “Sound emission and annihilations in a programmable quantum vortex collider,” *Nature* **600**, 64–69 (2021).
- [5] Mônica A. Caracanhas, Pietro Massignan, and Alexander L. Fetter, “Superfluid vortex dynamics on an ellipsoid and other surfaces of revolution,” (2021), [arXiv:2110.13560](#).
- [6] M. R. Matthews, B. P. Anderson, P. C. Haljan, D. S. Hall, C. E. Wieman, and E. A. Cornell, “Vortices in a bose-einstein condensate,” *Phys. Rev. Lett.* **83**, 2498–2501 (1999).
- [7] M. R. Matthews, B. P. Anderson, P. C. Haljan, D. S. Hall, M. J. Holland, J. E. Williams, C. E. Wieman, and E. A. Cornell, “Watching a Superfluid Untwist Itself: Recurrence of Rabi Oscillations in a Bose-Einstein Condensate,” *Phys. Rev. Lett.* **83**, 3358–3361 (1999).
- [8] E. Nicklas, W. Muessel, H. Strobel, P. G. Kevrekidis, and M. K. Oberthaler, “Nonlinear dressed states at the miscibility-immiscibility threshold,” *Phys. Rev. A* **92**, 053614 (2015).
- [9] A. Farolfi, A. Zenesini, D. Trypogeorgos, C. Mordini, A. Gallemí, A. Roy, A. Recati, G. Lamporesi, and G. Ferrari, “Quantum-torque-induced breaking of magnetic interfaces in ultracold gases,” *Nat. Phys.* (2021),

- 10.1038/s41567-021-01369-y.
- [10] A. Farolfi, A. Zenesini, R. Cominotti, D. Trypogeorgos, A. Recati, G. Lamporesi, and G. Ferrari, “Manipulation of an elongated internal Josephson junction of bosonic atoms,” *Phys. Rev. A* **104**, 023326 (2021), [arXiv:2101.12643](#).
- [11] D. T. Son and M. A. Stephanov, “Domain walls of relative phase in two-component Bose-Einstein condensates,” *Phys. Rev. A* **65**, 063621 (2002).
- [12] Juan J. García-Ripoll, Víctor M. Pérez-García, and Fernando Sols, “Split vortices in optically coupled Bose-Einstein condensates,” *Phys. Rev. A* **66**, 021602(R) (2002).
- [13] V. M. Kaurov and A. B. Kuklov, “Josephson vortex between two atomic Bose-Einstein condensates,” *Phys. Rev. A* **71**, 011601(R) (2005).
- [14] V. M. Kaurov and A. B. Kuklov, “Atomic Josephson vortices,” *Phys. Rev. A* **73**, 013627 (2006).
- [15] Sophie S. Shamaïlov and Joachim Brand, “Quasiparticles of widely tuneable inertial mass: The dispersion relation of atomic Josephson vortices and related solitary waves,” *SciPost Phys.* **4**, 018 (2018), [arXiv:1709.00403](#).
- [16] Kousuke Ihara and Kenichi Kasamatsu, “Transverse instability and disintegration of a domain wall of a relative phase in coherently coupled two-component Bose-Einstein condensates,” *Phys. Rev. A* **100**, 013630 (2019), [arXiv:1904.02380](#).
- [17] A. Gallemí, L. P. Pitaevskii, S. Stringari, and A. Recati, “Decay of the relative phase domain wall into confined vortex pairs: The case of a coherently coupled bosonic mixture,” *Phys. Rev. A* **100**, 023607 (2019), [arXiv:1906.06237](#).
- [18] Minoru Eto, Kazuki Ikeno, and Muneto Nitta, “Collision dynamics and reactions of fractional vortex molecules in coherently coupled Bose-Einstein condensates,” *Phys. Rev. Research* **2**, 033373 (2020).
- [19] Shigehiro Yasui and Muneto Nitta, “Domain walls in neutron 3p_2 superfluids in neutron stars,” *Phys. Rev. C* **101**, 015207 (2020).
- [20] Michikazu Kobayashi and Muneto Nitta, “Proximity effects of vortices in neutron 3p_2 superfluids in neutron stars: Vortex core transitions and covalent bonding of vortex molecules,” (2022), [10.48550/ARXIV.2209.07205](#).
- [21] Kenichi Kasamatsu, Makoto Tsubota, and Masahito Ueda, “Vortex Molecules in Coherently Coupled Two-Component Bose-Einstein Condensates,” *Phys. Rev. Lett.* **93**, 250406 (2004).
- [22] Minoru Eto and Muneto Nitta, “Confinement of half-quantized vortices in coherently coupled Bose-Einstein condensates: Simulating quark confinement in a QCD-like theory,” *Phys. Rev. A* **97**, 023613 (2018).
- [23] Mattia Cipriani and Muneto Nitta, “Crossover between Integer and Fractional Vortex Lattices in Coherently Coupled Two-Component Bose-Einstein Condensates,” *Phys. Rev. Lett.* **111**, 170401 (2013).
- [24] Marek Tylutki, Lev P. Pitaevskii, Alessio Recati, and Sandro Stringari, “Confinement and precession of vortex pairs in coherently coupled Bose-Einstein condensates,” *Phys. Rev. A* **93**, 043623 (2016).
- [25] Luca Calderaro, Alexander L. Fetter, Pietro Massignan, and Peter Wittek, “Vortex dynamics in coherently coupled Bose-Einstein condensates,” *Phys. Rev. A* **95**, 023605 (2017).
- [26] Sarthak Choudhury and Joachim Brand, “Rotational pendulum dynamics of a vortex molecule in a channel geometry,” *Phys. Rev. A* **106**, 043319 (2022).
- [27] Lauriane Chomaz, Laura Corman, Tom Bienaimé, Rémi Desbuquois, Christof Weitenberg, Sylvain Nascimbène, Jérôme Beugnon, and Jean Dalibard, “Emergence of coherence via transverse condensation in a uniform quasi-two-dimensional Bose gas,” *Nat. Commun.* **6**, 6162 (2015), [arXiv:1411.3577](#).
- [28] C. J. Pethick and H. Smith, *Bose-Einstein Condensation in Dilute Gases* (Cambridge University Press, Cambridge, UK, 2008).
- [29] P. G. Saffman, *Vortex Dynamics* (Cambridge University Press, Cambridge, 1995).
- [30] Jonathan Skipp, Jason Laurie, and Sergey Nazarenko, “Hamiltonian derivation of the point vortex model from the two-dimensional nonlinear Schrödinger equation,” (2022), [arXiv:2208.10412](#).
- [31] L. A. Toikka and J. Brand, “Asymptotically solvable model for a solitonic vortex in a compressible superfluid,” *New J. Phys.* **19**, 023029 (2017), [arXiv:1608.08701](#).
- [32] A. S. Bradley, “Vortexdistributions.jl,” (2022).
- [33] Paul K. Newton, *The N-Vortex Problem*, Vol. 145 (Springer New York, New York, NY, 2001).